

Characterization of Fluvial-Eolian Aquifer Reservoirs: Integrating Digital Outcrop Models and GPR Data

Reginaldo Lemos ^{1*}, Manoela Bettarel Bállico ¹, Marcelo Accioly Teixeira de Oliveira ¹,
Felipe Guadagnin ², Monica de Oliveira Manna ³, Mariah Metzner ¹,
Amanda de Souza Carvalho Feitosa ¹, and Jean Carvalho Toledo ¹

¹Universidade Federal de Santa Catarina - UFSC, Florianópolis, SC, Brazil

²Universidade Federal do Pampa - Unipampa, Bagé, RS, Brazil

³Universidade Federal do Rio Grande do Sul - UFRGS, Porto Alegre, RS, Brazil

*Corresponding author email: regi.lemos@hotmail.com

ABSTRACT: The Rio do Rasto and Botucatu Formations represent the main aquifer reservoirs in the state of Santa Catarina Brazil. The vertical facies succession of these formations comprises reservoirs formed by a complex fluvial-eolian interaction. The analysis of the depositional architecture, the use of geophysical data and of high-resolution virtual outcrop models from these reservoirs improved the understanding and of high-resolution heterogeneities at different scales and allowed the development of lithological and aquifer models that demonstrate this interaction. At megascopic scale, the reservoirs are composed of fine-grained sediments interbedded with sandy bodies deposited in a fluvio-eolian context of the Rio do Rasto Formation, and large-scale eolian dunes deposited in a dry eolian system of the Botucatu Formation. At macroscopic scale, the fluvial-interpreted reservoir presented more vertical and lateral heterogeneities relative to the eolian reservoir. Unconformity surfaces and clay layers act as its main flow barriers. At mesoscopic heterogeneity reflects lithofacies and sedimentary structures within eolian and fluvial facies associations. In this scale the major parameters that impact the flow migration are textural and structural differences associated with eolian and fluvial depositional processes.

Keywords: fluvial-eolian reservoirs; Rio do Rasto Formation; Botucatu Formation; multi-scale heterogeneities

INTRODUCTION

Deposits originating from fluvial-eolian systems constitute important water/oil/gas reservoirs due to their high permeability and porosity characteristics (Riccomini et al., 2012). However, these reservoirs present diverse depositional (textural intercalations, types of stratification and layer architecture) and/or post-depositional (compaction, cementation and tectonic deformations) heterogeneities (Galloway and Hobday, 1996), which can compartmentalize and make them unproductive.

To understand these heterogeneities at their different scales (micro, meso and macro) and their relationships with petrophysical parameters (porosity and permeability), various data are needed, such as stratigraphic profiles, wells, geophysical surveys, as well as digital aerial photogrammetry to generate

digital models of outcrops (DOM).

Among the equipment that allows acquiring such data, GPR and the use of Remotely Piloted Aircraft (RPA's) stand out, which have the capacity to provide images of features in high-resolution (cm scale), in shallow subsurface (up to 100 meters in depth) and surface, mainly in outcrops that are difficult to access.

Research involving the application of the GPR method is found in several authors such as: Davis and Annan (1989), Pringle et al. (2004), Neal (2004), Forte et al. (2012), De Oliveira et al. (2020). In the context of siliciclastic rocks of river and wind environments, we highlight the work of Bristow et al. (1996); Van Overmeeren (1998); Bristow et al. (2000; 2005), Neal and Roberts (2001), Lee et al. (2007), Botha et al. (2003), Bongiorno and Scherer (2010); Souza (2013), Bállico et al. (2017), Magalhães et al. (2017). The works that address the characterization of reservoir heterogeneities based on MVA can be found in Eltom et al. (2017), Massaro et al. (2018); Kroth (2018); Howell et al. (2014), Roisenberg (2020) and Thomas et al. (2021).

The State of Santa Catarina is made up of successions of hydrostratigraphic units that represent geological domains from the Precambrian to the Cenozoic (Machado, 2013). Among them, the Rio do Rasto and Botucatu formations stand out. The Rio do Rasto Hydrostratigraphic Unit occurs along the band of outcrops of Gondwana sedimentary rocks, in lower contact with the Teresina Unit, and in its upper portion in contact with the Botucatu Hydrostratigraphic Unit. That unit is characterized by presenting different lithological sets, which are subdivided into the Serrinha and Morro Pelado Members (Machado, 2013).

In general terms, the Serrinha Member is made up of fine, well-sorted sandstones, interspersed with gray-green, brownish, burgundy and reddish siltstones and mudstones, and may locally contain lenses or horizons of marly limestone; Morro Pelado, they are made up of lenses of fine, reddish sandstones, interspersed with purplish siltstones and mudstones (Machado, 2013).

The Botucatu Hydrostratigraphic Unit makes up the Guarani Aquifer System (GAS), which is composed of the Piramboia and Botucatu Formation (Rebouças, 1976). Because of its high porosity, permeability, homogeneity, continuity and dimensions, the (GAS) is considered one of the largest aquifer systems in the world (Machado, 2013). However, the contrast between the fluvial/lacustrine lithologies of the Piramboia Formation and the eolian lithologies of Botucatu may confer a certain anisotropy and heterogeneity to the (GAS). Given this, and because the (GAS) behaves like a multi-layer aquifer, based on the conception of a large aquifer system, it has an unknown architecture on a macro scale, as well as the influence it can exert on its reserves and water quality (Machado, 2013). This author also highlights that the existence of tectonic compartmentalization into blocks generated by structural discontinuities makes it difficult to characterize it as a typical transboundary aquifer with continuous flow.

Among these lithologies, the sandstones of Botucatu Fm. are considered one of the best reservoirs in the (GAS), presenting an average porosity of 17% and hydraulic conductivity of 0.2 to 4.6 m/day

(Araújo et al., 1995). Deposited in an aridization context, this formation presents records of eolian deposits associated with extensive ergs (dune fields) of Jurassic-Cretaceous age (Milani et al., 2007; Warren et al., 2008; Soares; Soares; Holz, 2008). From a compositional point of view, Botucatu Fm. is mainly made up of fine-to medium-grained quartz sandstones, whitish, yellowish and pink in color, well selected, regularly classified, silt-clay, quartz, with subrounded grains (Milani et al., 2007, Machado, 2013). In this context, the present work aims to differentiate, using GPR and aerial photogrammetry, internally and externally the depositional architecture of the fluvial-eolian systems of the Rio do Rasto and Botucatu formations, individualizing the connections, compartmentalizations and the main associated heterogeneities

STUDY AREA LOCATION

The geological interval under study is located near the municipalities of Lages and Painel, located in the Santa Catarina Plateau region, **Figure 1**. Three specific areas were selected for the development of the research: Area I, located adjacent to SC-114 highway, towards the city of Painel, where the Rio do Rasto and Botucatu formations are mapped; Areas II, located near Devil's Throat River.

Geomorphologically, the areas are located on the SE margin of the Lages Dome. This structure has a concentric geometry, slightly elongated in the NW-SE axis, whose uplift and erosion, due to the intrusion of alkaline magmatism into the structure, exposed stratigraphic units of Permian and Early Cretaceous age, such as Rio do Rasto and Botucatu formations (Scheibe, 1986).

GEOLOGICAL SETTING

The Paraná Basin is an intracratonic basin that covers an area of approximately 1,400,000 km², of which 1,100,000 km² are on Brazilian territory, with the remainder distributed between Paraguay, Argentina and Uruguay (Bergamaschi, 1999, Milani et al., 2007). The geometric shape of the basin resembles an ellipse with a major axis N-S, whose evolution took place during the Paleozoic and Mesozoic, starting from a gulf open to the Panthalassa Ocean and later becoming an intracratonic depression due to the convergent movement between Gondwana and the oceanic crust (Milani et al., 2007).

The basin is filled by a sedimentary-magmatic package, approximately seven thousand meters long, deposited between the Late Ordovician and the Late Cretaceous (Milani et al., 2007). Six second-order allostratigraphic units or supersequences are recognized in it, individualized by interregional unconformity surfaces (Milani, 1997), these units are: 1) Rio Ivaí (Ordovician-Silurian); 2) Paraná (Devonian); 3) Gondwana I (Carboniferous-Eotriassic); 4) Gondwana II (Meso to Neo-Triassic); 5) Gondwana III (Neo-Jurassic-Eocretaceous); and 6) Bauru (Neo-Cretaceous). The first three supersequences (Rio Ivaí, Paraná and Gondwana I) record cycles of transgression of sea level regression in the Paleozoic, while the last three Gondwana II, Gondwana III and Bauru) are formed by continental sedimentary sequences (Mesozoic) and association of igneous rocks. Which, the Gondwana I and III

supersequence include the Rio do Rasto and Botucatu Formation respectively.

The Rio do Rasto Formation has a maximum thickness of 600 m (Scherer et al., 2023) and can be further subdivided into the Serrinha and Morro Pelado Member. The Serrinha Member, with a thickness ranging from 150 to 250 meters, primarily consists of siltstones and fine sandstones. In contrast, the Morro Pelado Member, with a thickness of 250 to 300 meters, is composed of fine to medium sandstones, siltstones, and secondary reddish mudstones (Holz et al., 2010).

Deposited in an arid environmental context, the Morro Pelado Member is predominantly characterized by creamy yellowish, purplish and reddish siltstones and sandstones with lenticular and sigmoidal geometry, its thickness can vary from decimetric to metric (Rohn, 1994, Meghioratti, 2006, Warren et al., 2008, Holz et al., 2010, Schemiko et al., 2014, Alessandretti et al., 2015). Due to this association, several depositional paleoenvironments have been proposed, however, there is a consensus that the deposition of the Morro Pelado Member occurred in more arid circumstances associated with continental systems (Lavina, 1991; Rohn, 1994; Warren et al., 2008; Holz et al., 2010; Schemiko et al., 2014; Alessandretti et al., 2015; Azevedo, 2018; Toledo et al., 2023).

Botucatu Fm. is composed of fine to medium, and occasionally coarse, well-sorted light sandstones, with rounded, highly spherical grains with large to small channeled or planar cross-stratifications (Scherer, 2000; Da Silva and Scherer 2000; Soares; Soares; Holz, 2008). A facies study carried out by Scherer (2000) indicates that the main dune morphologies related to Botucatu Fm. are simple crescents, compounds and complex linear draas. According to Soares; Soares and Holz (2008), the origin of this formation dates back to extensive ergs associated with desert subenvironments, indicated by wadis deposits, with basal rudaceous facies and lacustrine deposits indicated by laminated pelitic facies. Previous studies indicate that the direction of sand transport and dune migration occurred to the northeast, suggesting that the source area was to the west/southwest (Bigarella and Salamuni, 1961; Scherer, 1998).

The Botucatu Fm. is limited at the base by a regional unconformity developed on the fluvio-lacustrine deposits of the Rio do Rasto Fm. while the upper contact is concordant with Serra Geral Fm. (Da Silva and Scherer, 2000). According to Gordon Jr. (1947), this basal unconformity highlights the limit between the Paleozoic and Mesozoic eras. However, the contact relationship with the underlying units is still a topic of discussion and there are different interpretations for each location, as discussed by Soares; Soares and Holz (2008).

In the study area, the Morro Pelado Member is composed of 15 lithofacies, **Table 1** and **Figure 2**, that were grouped into five architectural elements, characterizing this unit as distributive fluvial systems in a terminal context, while the Botucatu Formation is dominated by two lithofacies, **Table 1** and **Figure 3**, being interpreted as dry eolian systems (Scherer, 1998 and 2000).

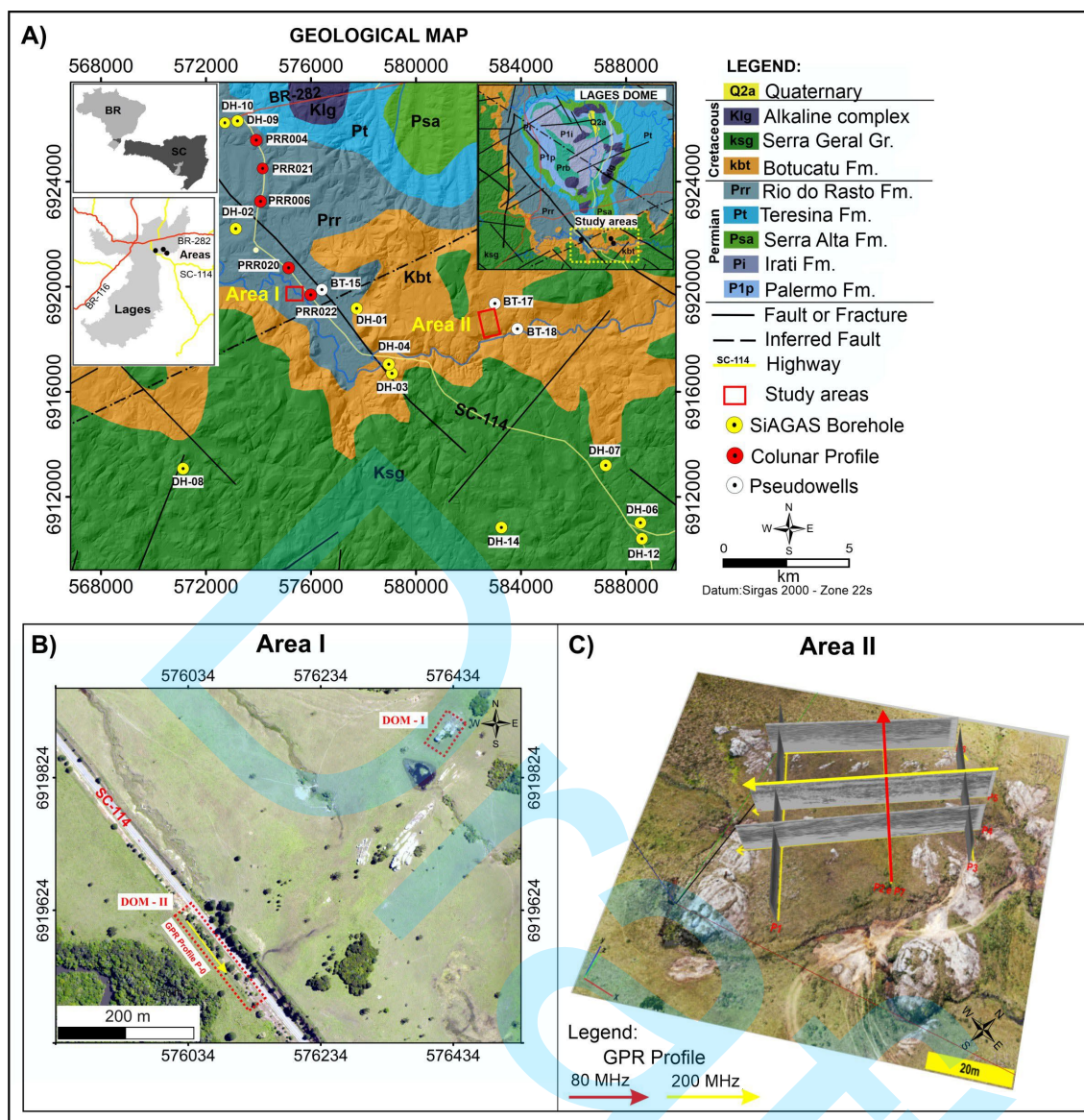


Figure 1. A) Geological Map; B and C) aerial images of the areas surveyed and with the overlap of the GPR sections

Table 1. Lithofacies of the Rio do Rasto and Botucatu formations recognized in the study area and characterized in terms of lithology, texture, sedimentary structure, and other depositional and post-depositional features (Adapted from Miall, 1996). The lithofacies codes with (e) indicate eolian processes.

Litofacies Code	Description	Interpretation
Gcm	Granule- to pebble-supported massive, intraformational conglomerates. Poorly sorted, fine to very coarse-grained sandy matrix with subangular to subrounded mudclasts. Presents erosive basal surface.	High-energy flows, hyperconcentrated in sediments and eroded floodplain mudclasts (Miall, 1996).

Sm	Poorly to moderately sorted, massive, very fine- to fine-grained sandstones.	High-energy flows, hyperconcentrated in sediments (Miall, 1996).
Slu	Moderately sorted, very fine-grained sandstones with slightly undulated horizontal lamination.	Deposition under in-phase, non-breaking waves in upper flow regime conditions and highly aggradational settings (Cartigny et al., 2014).
Sl	Moderately sorted, very fine- to fine-grained sandstones with low-angle cross-stratification.	Transitional flow conditions between upper plane-bed and antidunes stability fields (Fielding, 2006).
St	Moderately sorted, fine-grained sandstones with trough cross-stratification.	Unidirectional, subaqueous migration of sinuous-crested dunes (Miall, 1996).
Sr	Moderately sorted, very fine-grained sandstones with small-scale, ripple cross-lamination with critical to supercritical climbing angle. Laminae may be deformed.	Small-scale, sinuous-crested bedforms deposited by lower regime flow, combining traction and suspension processes (Miall, 1996). Laminae deformation may occur due to bioturbation or fluid scape.
Sw	Moderately to well- sorted, very fine-grained sandstone with wavy, low-angle truncated cross-lamination.	Small-scale bedforms deposited and reworked by wind-induced oscillatory currents (Plint et al., 2010).
Sd/S?	Poorly to moderately sorted, very fine- to fine-grained sandstones with no distinguished sedimentary structure.	Completely indistinguishable strata or laminae deformation due to pedogenesis, intense bioturbation, or fluid scape.
Ht	Heterolithic bedding characterized by millimeter- to centimeter-scale intercalation of moderately sorted, very fine-grained, massive, undulated or rippled cross-laminated sandstones and massive to laminated siltstones to mudstones. Laminae may be deformed.	Intercalation of traction and suspension processes (Reineck and Singh, 2012). Laminae deformation may be associated with bioturbation, pedogenesis, or mud shrinkage under subaerial conditions.
Fl	Purple to red siltstones and claystones with horizontal laminae. Laminae may be deformed.	Gravitational setting of fine-grained sediments under low energy conditions. Laminae deformation may be associated with bioturbation, pedogenesis, or mud shrinkage under subaerial conditions (Miall, 1996.).
Fm	Purple to red, massive sandy siltstones, siltstones and claystones.	
P	Purple to red very fine-grained sandstones, sandy siltstones, and siltstones with poorly-developed pedogenetic features.	Non-depositional intervals and early pedogenetic processes under subaerial exposure (Retallack, 1976).
St(e)	Moderately to well- sorted, very fine- to fine-grained sandstones with subangular to rounded grains. Trough cross-strata consist of bimodal, millimetrically-spaced, inversely graded pin-stripe lamination eventually intercalated with millimetric to centimetric structureless laminae.	Migration of eolian dunes dominated by translantent wind ripples alternating with grain fall settling, located at the base of the dune (Hunter, 1977; Kocurek, 1991).
Sl(e)	Moderately to well-sorted, very fine- to fine-grained sandstones with subangular to rounded grains with low-angle, millimetrically-spaced, bimodal, inversely graded pinstripe laminae.	Migration of translantent wind ripples (Hunter, 1977).
Sa(e)	Sandy siltstones to moderately to well-sorted, very-fine grained sandstones with crenulated horizontal laminae.	Adhesion of dry sand to a wet or damp surface (Kocurek and Fielder, 1982).

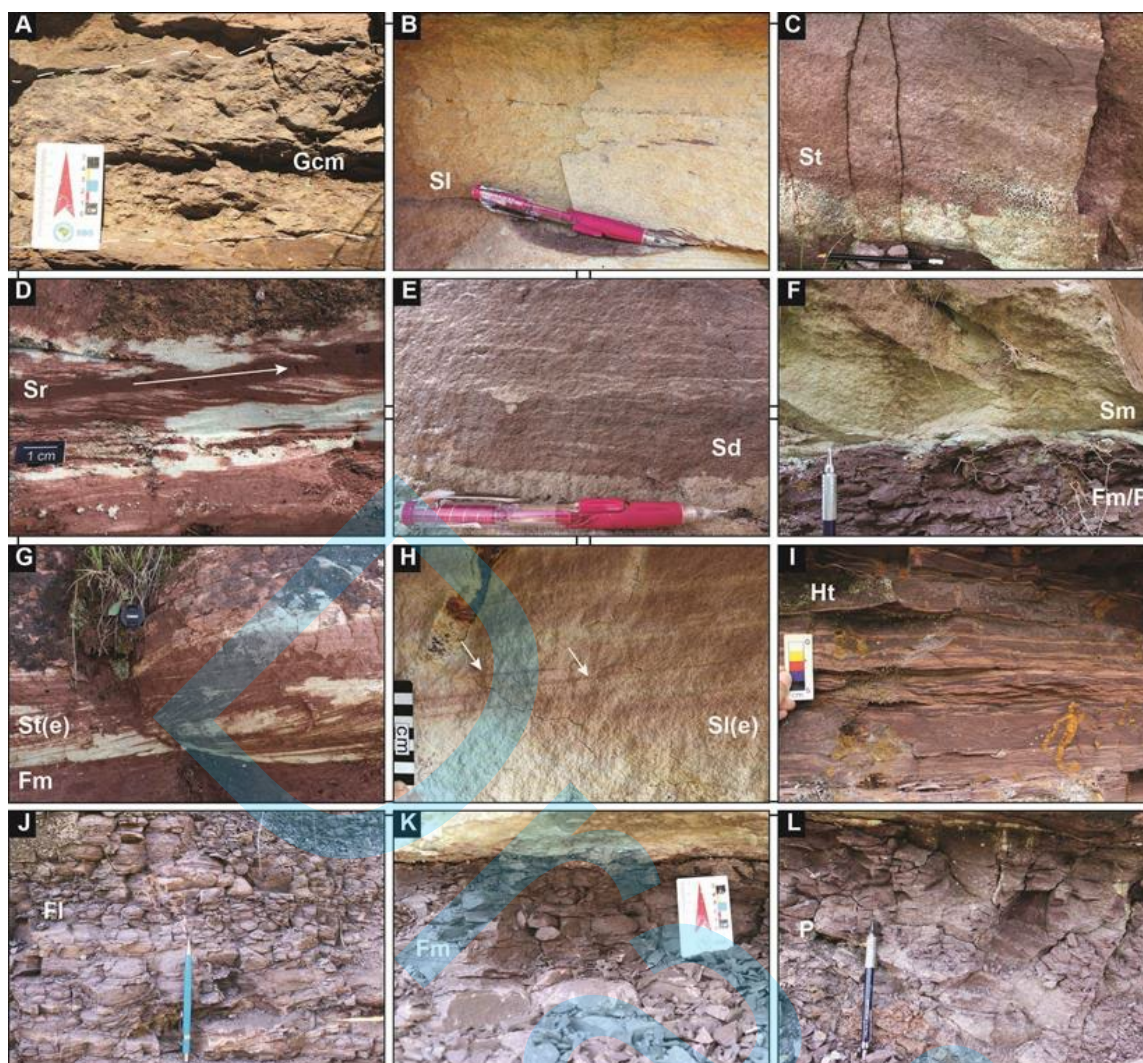


Figure 2. Field photographs representing each sedimentary facies of the study area. See description and interpretation in the Table 1. (A) Lenticular beds of intraformational conglomerates with granule and pebble-sized muddy and sandy intraclasts; (B) Moderately sorted, low-angle cross-stratified fine-grained sandstone, with elongate silty intraclasts; (C) Moderately sorted, trough cross-stratified fine-grained sandstone; (D) Ripple cross-lamination with climbing angle within silty very fine-grained sandstone; (E) Moderately sorted, fine-grained sandstone with indistinct syn-depositional structures; (F) Well-sorted, massive, very-fine grained sandstone in contact with purple, massive, blocky mudstone; This contact is typically marked by a greenish bend; (G) Stacked trough cross-stratified sets of well-sorted, very fine-grained sandstones composed of translantent wind ripple strata; (H) Well-sorted, fine-grained sandstone composed of low-angle cross-stratification of translantent wind ripple strata; (I) Heterolithic beds with variable proportions of sand and mud, consisting of millimeter- to centimeter-scale intercalated massive to wavy ripple cross-laminated very fine to fine-grained sandstones and laminated to massive mudstones; These beds typically show pronounced degrees of bioturbation; (J) Purple to pinkish purple wavy to horizontally laminated mudstones with occasional bioturbation; (K) Purple massive mudstone with occasional bioturbation; (L) Purple mudstone with blocky texture, greenish mottling and thin, grayish haloed rootmarks.

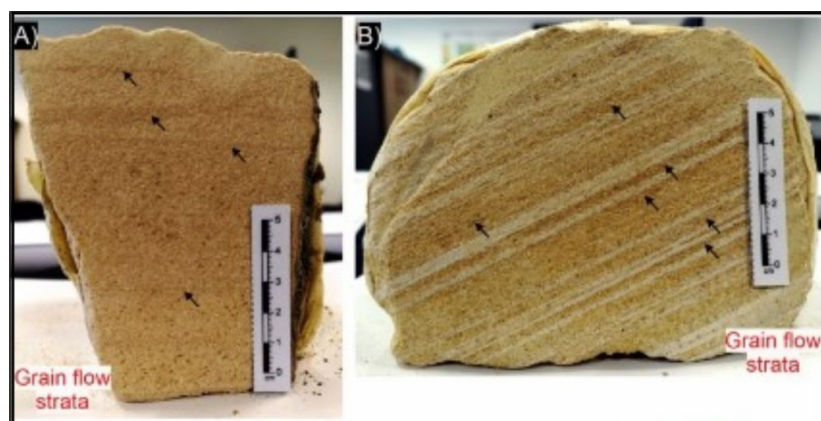


Figure 3. The main sedimentary structures on eolian dunes facies association. A and B) Intercalation relationship between grain flow and translational laminations

METHODS

GPR Acquisitions in the Study Area

In addition to detailed stratigraphic loggings, surveying and mapping using Digital Outcrop Models (DOMs), 3D digital modelling of the outcrops and geophysical investigations using with Ground Penetrating Radar (GPR) have been used. The main focus of this methodology is on the description of sedimentary structures and architectural elements that form fluvio-eolian reservoirs.

The geophysical survey was carried out with GPR equipment from GSSI (Geophysical Survey Systems Inc.), using an antenna at a frequency of 200 MHz and an unshielded low-frequency antenna (80 MHz). Fourteen GPR profiles were acquired. Twelve in the Area 2 (ten at 200 MHz and two at 80 MHz, and two profiles in Area 1 (200 MHz), **Figure 1**. Data was acquired following the common-offset acquisition method. Data is post-processed by RADAN 7.0® and ReflexW 3® softwares in order to increase the signal to noise ratio by applying of high-pass and low-pass filters; time-variant scale gain; Kirchhoff migration, and topographic correction, following basic standard post-processing routines (Neal, 2004). GPR data are presented as GPR profiles, or radargrams. Ground truth data were obtained for GPR profiles above rock outcrops, enabling for calculation of dielectric constants by converting two-way travel-times primary data into average velocities of radio pulses propagation. The radargrams may then be interpreted in terms of actual depths. The calculated dielectric constants (K), for this study range from 6 to 10. These constants also known as the relative permittivity (ϵ_r), is a dimensionless quantity that represents how much a material can store electrical energy compared to a vacuum. Mathematically it is defined as: $\epsilon_r = \epsilon/\epsilon_0$, where ϵ = dielectric permittivity of the material (farads/meter - F/m) and ϵ_0 = dielectric permittivity in vacuum (8.854×10^{-12} F/m).

The average propagation velocities in the surveyed subsoil range from 0.12-0.09 meters per nanoseconds, respectively. General principles of GPR stratigraphy, derived from seismic stratigraphy, are applied to the description of subsurface structures (sediments and rocks), as revealed by GPR reflectors (Neal, 2004).

Acquisition and Processing of Aerial Images

A DJI Phantom 4 RPA with integrated camera and Global Navigation Satellite System were used in this study. This model has a camera coupled with Complementary Metal-Oxide Semiconductor (CMOS) sensors, measuring approximately 11 mm, which allows photos to be taken with a resolution of 12 megapixels (4000 x 3000) and a pixel size of 1.55 x 1.55 μm . It has a 20 mm lens, equivalent to the 35 mm format, with a focal length of 3.61mm and a 94° field of view.

The aerial images acquisition was carried out in two stages. In the first, the flight plan was programmed to take photos at an altitude of 70 m above ground. This acquisition was planned using the UgCS software based on topographic information from the Shuttle Radar Topographic Mission (SRTM). The objective of this first flight plan was to obtain a higher resolution Digital Elevation Model (DEM) for planning a second flight at a lower altitude. The second phase of acquisition was based on the DEM from the previous field trip, with a programmed plan to acquire images at 15.6 and 20 m altitude for Digital Outcrops Models (DOM's) 1 and 2.

The aerial photographs were processed using Metashape Photoscan 1.4.2 software. This software allows the application of the SfM-MVS workflow. Therefore, the processing of the aerial images follows, as a reference, the workflow presented by Viana et al. (2018) and Pasetto et al. (2020). The processing flow consists of five main steps: 1st) selection and alignment of photos; 2nd) generation of point cloud (sparse and/or dense); 3rd) creation of Digital Surface Models (DSM) and Digital Terrain Models (DTM); 4th) application of texture to improve the visual aspect of the model; 5th) creation of Digital Outcrop Model (DOM).

The alignment of the photographs and the generation of the sparse point cloud were carried out in a high quality using all of the photographs. The dense point cloud was then constructed points, at this stage the software increases the number of reconstructed points by two or three orders of magnitude, in relation to the sparse point cloud; then it is possible to build the triangulated surface (mesh) and finally generate the texturing of the model. All these steps were carried out with high quality, allowing the generation of models with resolutions of 8 mm and 2.54 cm per pixel for DOM's I and II respectively.

Generation of Lithological and Aquifer Modeling

This approach involved developing 3D facies models and relating these models to hydrostratigraphic units and aquifer types. The method used in this work employs lithological modelling techniques based on the concept of "solid modelling" concept of RockWorks 15 software, using a kriging algorithm. This method allows the prediction of measurements and observations in places where the value of the variable is unknown based on previously collected data.

The models were developed based on data from 10 boreholes, available on the website of the Secretariat for Economic Development of the State of Santa Catarina (SDE/SC). These boreholes were selected on the basis of proximity and because they are more geologically representative of the study area. The well database contains information on the location, depth, groundwater level and flow rate,

lithology, sediment texture, and elevation. In addition, eight simulated boreholes (pseudowells) were created to adjust the model; five were obtained from columnar profiles surveyed in the area by Manna et., al *in prep.*, and three were created from DOM's and GPR surveyed in this work,

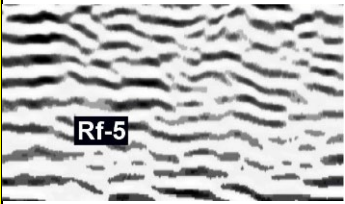
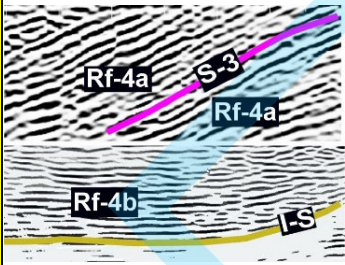
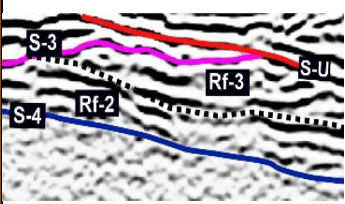
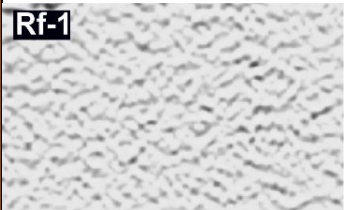
RESULTS AND DISCUSSION

Radar Facies and Surfaces

To standardize the identification of surfaces, stratigraphic packages, and sedimentary facies, we apply the principles of seismostratigraphy as outlined by Mitchum Jr. (1977) and Mitchum Jr. et al. (1977). These principles are based on the recognition of reflection patterns (including configuration, continuity, amplitude, and frequency) and reflection terminations or boundaries. In addition, we adopt the terminology proposed by Neal (2004). Radar surfaces are similar to boundary surfaces and represent depositional breaks or unconformities in the sedimentary sequence; radar packages are depositional units that consist of genetically related strata that are bounded at the base and top by radar surfaces or boundary surfaces; radar facies consist of sets of reflectors with distinct shape, dip and continuity that represent the bedding and internal structure of a given sedimentary facies.

In view of this and after processing the radargrams obtained with the 200 and 80 MHz antennas, it was possible to individualize a total of five radar facies and four boundaries surfaces as follows (**Table 2**): radar facies Rf-1, Rf-2 and Rf-3 were associated with the Morro Pelado Member (Rio do Rasto Fm.); radar facies Rf-4a, Rf-4b and Rf-5 were related to Botucatu Formation. The S-U corresponds to the unconformity surface that divides the units, the S-3 are the internal surfaces of the radar facies Rf-3 and Rf-4a, The Interdune Surface (I-S) corresponds to the basal surfaces bounding the radar facies Rf-4a, Rf-4b and Rf-5; S-4 occurs between R-f-1, Rf-2 and Rf-3, and divides distinct depositional units. The results and discussions of this work are presented according to the hierarchical orders, from a stratigraphic point of view, and the radar facies identified in each study area.

Table 2. Description and interpretation of the radar facies and boundary surfaces.

	Radar Facies and Surfaces	Description	Interpretation
Botucatu Fm.		Characterized by subhorizontal reflectors (maximum dip of 5°) with moderated continuity and amplitude signal, laterally extensive (more than 75 meters). These radar facies are truncated by high-amplitude subhorizontal (I-S) reflectors.	Subhorizontal reflectors suggest sets with low-angle cross-stratification. From the surface outcrop, this radar facies corresponds to low-angle inclined wind-ripple strata. The predominance of climbing translent strata suggests deposition by wind ripples in an interdune context, sandsheets or dune plinth deposits.
		Sigmoidal to tangential reflectors with dip angles varying between 25° and 28° in the NW direction. Internally, reflectors can be subdivided into sub-sets, which are themselves bounded by inclined surfaces (S-3) that dip up to 25°. In the transverse profile. The Rf-4a present concave-upward reflections (Rf-4b) with strong amplitudes and good continuity.	The trough-tangential pattern of cross-stratification indicates deposition of 3D-crescentic bed forms. The inclined bounding surfaces (S-3) that occur internally within cross-bedded sets and which dip in a similar direction to the cross-strata are most readily interpreted as reactivation surfaces.
Rio do Rasto Fm.		Rf-3 comprises a low to medium amplitude, gently dipping reflections to 19°. Reflectors are organized in a thin wedge shaped, with dimensions of about 1.5 meters thick and 60 meters lateral extent, passing laterally to the radar facies Rf-1. The reflectors at the top are cut off by surface S-U.	The radar facies Rf-3 is interpreted as a set of cross-stratification. From the surface columnar profile these radar facies suggest deposition by migrating eolian dunes (Hunter, 1977).
		Rf-2 is characterized by sub-parallel, moderately inclined reflectors with good to moderated continuity and moderated amplitude signal. Rf-2 is structured in a tabular geometry, 1-meter thick and 30 m lateral extent. The reflectors at the base are cut off by surface S-4.	The presence of sub-parallel, moderately inclined reflectors with good to moderated continuity suggests horizontally stratified deposits. In correlation with the outcrop profile, this radar facies represents very fine-to fine-grained sandstones with low-angle cross-stratification interlayered with very fine-grained sandstones with adhesion structures.
		Rf-1 presents discontinuous and disorganized reflectors, sub-parallel to undulating, moderately inclined, with low-amplitude signal. The reflectors are truncated by the S-U and they end in tolap against the S-4.	The presence of discontinuous, disorganized reflectors indicates low resistivity deposits. In conjunction with the outcrop profile, it is possible to correlate this radar facies with laminated (facies Fl) and massive mudstones (facies Fm) and heterolithic deposits (facies Ht).

Rf - 1 Radar facies - Profile P - 0

Description: Rf-1 radar facies was identified only in Area I and is restricted to the basal part of the radargram (GPR Profile P-0), below 7.5 meters and over 126 m of surveyed profile, **Figure 4**. The radar facies present discontinuous and disorganized reflectors, sub-parallel to undulating, moderately inclined, with low-amplitude signal. The reflectors are truncated by the S-U and they end in tolap against the S-4. The low-amplitude of reflectors indicates a strong attenuation of GPR signal at the base of the profile. In general, the reflectors present a general preferential direction towards SE, dipping between 4° and 8° to Southeast/South.

Interpretation: The presence of discontinuous, disorganized reflectors indicates low resistivity deposits. In conjunction with the outcrop profile, it is possible to correlate this radar facies with laminated (Fl facies) and massive mudstones (Fm facies) and heterolithic deposits (Ht facies). The occurrence of the low-amplitude and signal attenuation at the base of the radargram indicates laterally extended beds. The sub-parallel to undulating southeast-dipping reflectors indicates the regional direction of the depositional surface.

Rf - 2 and Rf-3 Radar facies - Profile P - 0

Description: The radar facies Rf-2 was described in the Area I (GPR Profile P-0). This radar facies are characterized by sub-parallel, moderately inclined reflectors with good to moderated continuity and moderated amplitude signal. These radar facies are structured in a tabular geometry, 1 meter thick and 30 m lateral extent. The reflectors at the base are cut off by surface S-4 and are parallel to the surface above.

Interpretation: The presence of sub-parallel, moderately inclined reflectors with good to moderated continuity suggests horizontally stratified deposits. In correlation with the outcrop profile, this radar facies represents very fine-to fine-grained sandstones with low-angle cross-stratification interlayered with very fine-grained sandstones with adhesion structures, both facies resulting from eolian processes. This facies intercalation is associated with moderate amplitude reflectors **Rf-3** radar facies

Description: The **Rf-3** radar facies is restricted at Area I. Rf-3 comprises a low to medium amplitude, gently dipping reflections to 19°. Internally, this radar facies can be subdivided into sub-sets, which are themselves bounded by inclined surfaces that dip up to 15°. These surfaces truncate the reflector below but overlying reflector above is concordant. These reflectors are organized in a thin wedge shaped, with dimensions of about 1.5 m thick and 60 m lateral extent, passing laterally to the radar facies Rf-1, **Figure 4**.

Interpretation: Based on the signal characteristics, the radar facies Rf-3 is interpreted as a set of cross-stratification. From the surface columnar profile these radar facies suggest deposition by migrating eolian dunes (Hunter, 1977). The tangential pattern of cross-stratification indicates deposition of 3D-crescentic eolian dunes. According to outcrop profile, the foresets within trough cross-bedded

sets, inclined up to 19° are dominated by translent wind-ripple laminae, indicating that many dunes either lacked a significant active lee-side slipface (Mountney, 2006). The laterally discontinuous extent of the cross-bedded set that passing laterally into laminated mudstones (radar facies Rf-1) suggests that these small bedforms migrated and accumulated episodically and randomly as local accommodation became available. The inclined bounding surfaces that occur internally within cross-bedded sets and which dip in a similar direction to the cross-strata are most readily interpreted as reactivation surfaces (Surface S-3; Kocurek and Hunter, 1986).

Rf - 4a and Rf - 4b Radar facies – Profiles P - 0 and P - 7

Description: The radar facies Rf-4 occurs in the Area I (Rf-4a) and II (Rf-4a and Rf-4b), **Figure 4** and **Figure 5**. These radar facies present high-angle dipping reflections in the longitudinal profile (Rf-4a) and concave-upward reflections in the transverse profile (Rf-4b), with strong amplitudes and good continuity, **Figure 6**. The reflectors are large scale with 5-10 m thick and up to 70 m extent. In the longitudinal profiles, Profile P-0 - **Figure 4** and Profile P-7 - **Figure 5**. The Rf-4a reflectors show high-angle reflectors, dipping about 24° towards the Northeast. At the profile P-0 (Area I) the reflections downlap onto a low-angle reflection of the radar surface S-U, while in the Area II, the middle and uppermost of the profile P-7, **Figure 5**, the high-amplitude reflectors merge with lower-angle inclined reflectors, with low-amplitude, commonly in an intertonguing relationship, which they are bounded by slightly subhorizontal reflector. Internally, the reflectors are regularly punctuated by inclined bounding surfaces that dip at angles of 27° . In the transverse profile the radar facies Rf-4b contains concave-upward reflectors with moderate to good continuity, more than 60 meters long.

Interpretation: The presence of high-angle dipping reflections in the longitudinal profile (Rf-4a) and concave-upward reflections in the transverse profile (Rf-4b), **Figure 6**, correspond to sets of cross-stratification. These radar facies are consistent with the St(e) lithofacies of the Botucatu Formation, described in the DOM-I, **Figure 9**. The large, simple cross-bedded sets are interpreted to represent residual deposits of crescentic eolian dunes (Scherer, 2000). The high-angle and high-amplitude reflectors represent grainflow strata which indicate bedforms with well-developed slipfaces. The lower-angle inclined reflectors, with low-amplitude correspond to climbing translent wind ripples accumulated at the base of the dune. The frequent intertonguing of ripple strata with grainflow-grainfall strata suggest intervals during which sand was transported down the dune slopes as wind ripples, probably under the influence of winds oriented along the slope (Sweet and Kocurek, 1990; Sweet, 1992), before avalanche sedimentation resumed. The slightly subhorizontal reflector that bounded the high- and lower-angle reflectors, traced for several meters are interdune migration surface (I-S surface). The down-dipping boundary surfaces within these sets are examples of a type of reactivation surface formed as a result of episodic partial erosion of the lee slope of the bedforms (Brookfield, 1977; Fryberger et al., 1983).

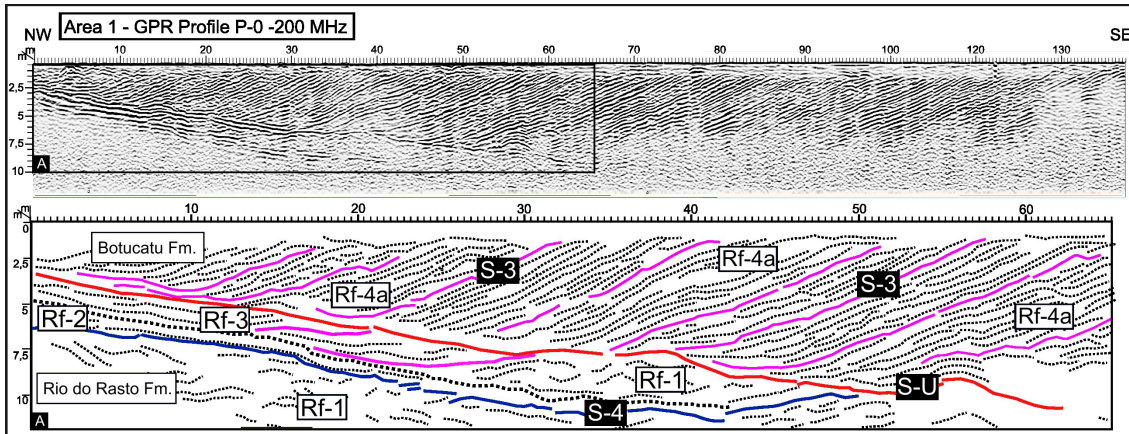


Figure 4. Post-processed radargram (Profile P - 0 - upper part) and interpretation of part of section A (indicated by the rectangle). This profile was obtained parallel to the structures and presents well-defined sigmoidal reflectors and limiting surfaces. Note the strong contrast between the radar facies. The S-4 and S-U correspond to the 4th order surface and unconformity surface, respectively.

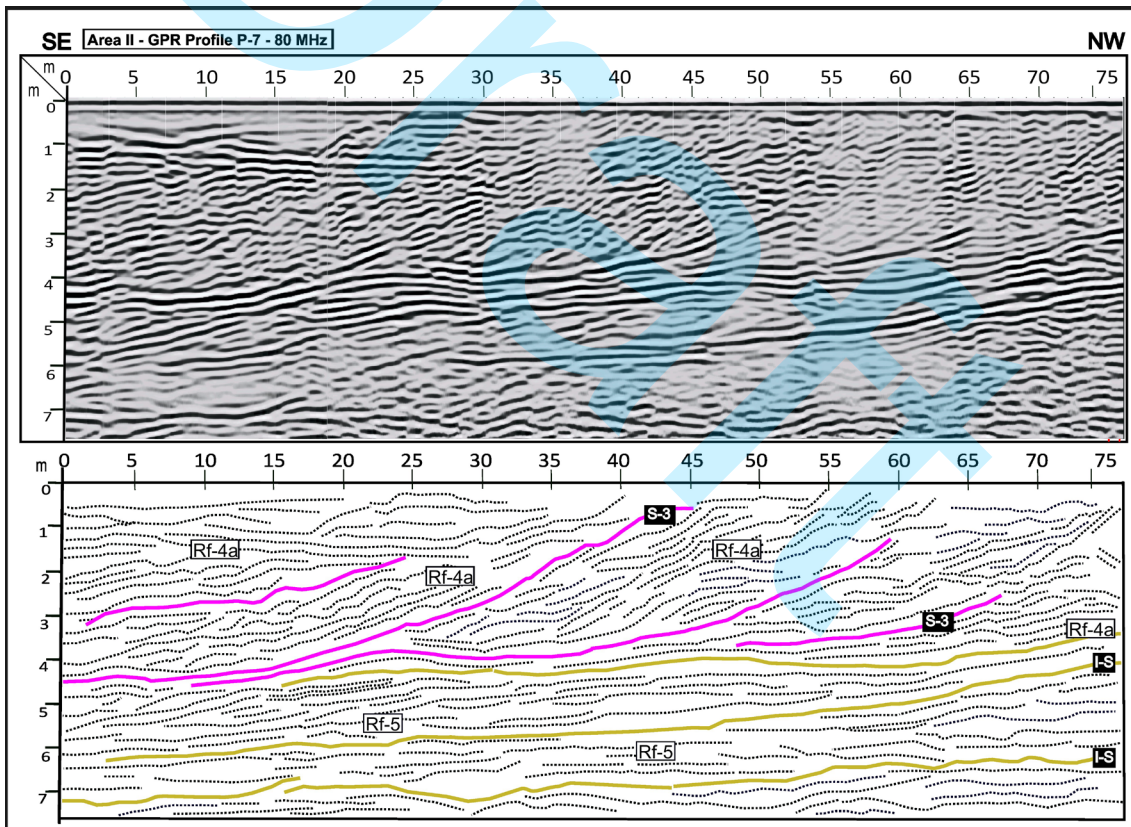


Figure 5. Post-processed radargram (Profile P - 7 - upper part) and interpretation. Note the change in the configuration of the Rf-5 and Rf-4a reflectors: I-S: Interdune surface (1st order) and S-3: 3rd order surface.

Rf - 5 Radar facies – Profiles P - 7 and P - 5

Description: The Rf-5 radar facies was identified in Area II, in profiles longitudinal to the direction of the dipping structures, using low frequency antennas (80 MHz). This radar facies are characterized by subhorizontal reflectors (maximum dip of 5°) with moderated continuity and amplitude signal, laterally extensive (more than 75 m), **Figure 6**. These radar facies are truncated by subhorizontal high-amplitude reflectors.

Interpretation: The presence of subhorizontal reflectors suggest sets with low-angle cross-stratification. From the surface outcrop, this radar facies corresponds to low-angle inclined wind-ripple strata. The predominance of climbing translantent strata suggests deposition by wind ripples in an interdune context, sandsheets or dune plinth deposits (Kocurek and Hunter, 1986; Clemmensen, 1989). The large lateral extent of the reflectors and the relation between this radar facies to the Rf-4 radar facies suggest dune plinth deposits. The subhorizontal high-amplitude reflectors truncating the Rf-5 radar facies is the interdune surface (I-S surface).

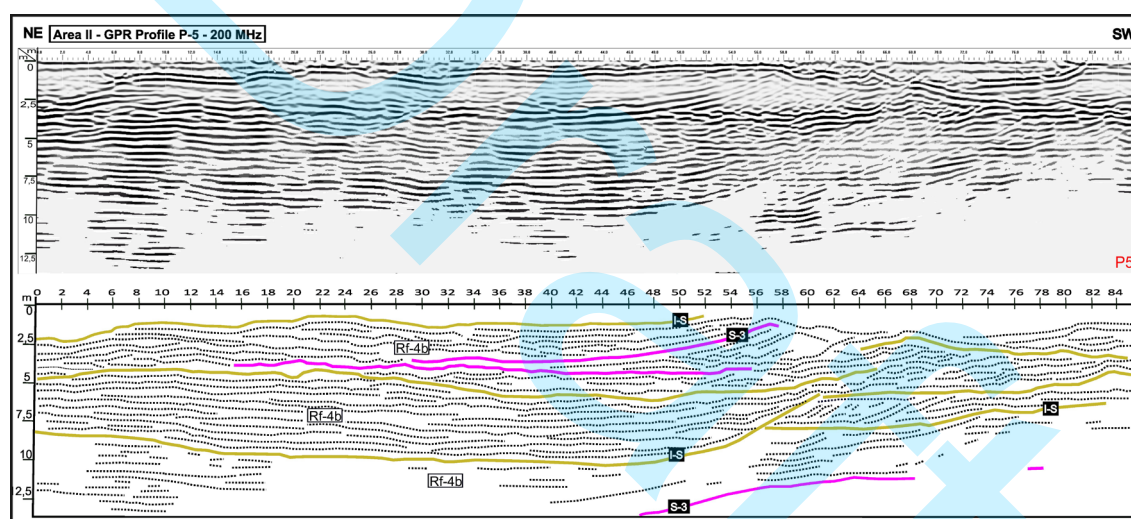


Figure 6. The processed GPR Profile P - 5 (upper part) and interpretation. This profile was obtained transversally to the structures and displayed the well-defined concave reflectors of the Rf-4b radar facies and the surfaces: IS: Interdune surface (1st order) and S-3: 3rd order surface.

ARCHITECTURAL ELEMENTS

The architectural elements were based on the outcrop description combined with the radar facies. Based on the different internal organization of reflectors of each radar facies and boundary surface, three architectural elements were distinguished, two for Morro Pelado Member and one for Botucatu Fm.

Morro Pelado Member (Rio do Rasto Formation): Floodplain Deposits

Description: These deposits are characterized by tens of meters of laterally extensive, sharp-bedded, tabular to wedge-shaped siltstones, mudstones, claystones, and paleosols 0.1 to 3 m thick. The

lithofacies of the floodplain deposits include dominantly red to purple massive and blocky to horizontally laminated fine-grained rocks (Fm and Fl, respectively). Paleosols (P) are characterized by poorly to moderately developed weathering profiles with slickensides, peds, redoximorphic features, root traces/marks, and few carbonate concretions. Heterolithic (Ht) beds are common. These heterolithic beds show millimeter- to centimeter-scale laminations of massive to wavy cross-laminated very fine-grained sandstones and fissile mudstones, mudcracks are also common.

Interpretation: Laterally extensive tabular beds of fine-grained rocks are found in floodplains characterized by low-lying alluvial areas prone to river inundation where subsequent water stagnation causes sediment deposition by gravitational settling (Miall, 1996; Marriott and Alexander, 1999). In addition, topographic depression, subaerial exposure, and the frequency and intensity of flood events contribute to the highly variable aspects of floodplain fines. Fine-grained rocks and poorly developed paleosols (< 0.5 m) are dominated by redoximorphic features, attesting to intervals of water accumulation (Gulliford et al., 2017). Heterolithic beds and horizontally laminated mudstones may be associated with floodplain lakes that developed during paleotopographic lowstands.

Morro Pelado Member (Rio do Rasto Formation): Sandsheets and Eolian Dunes

Description: This deposit consists of bimodal, moderately to well-sorted, very fine-to medium-grained sandstones arranged in tabular bodies up to 2m-thick and tens of meters wide, **Figure 7 and Figure 8**. Internally, these sandbodies are composed of 1 to 2 m thick sets of low-angle (<5°) cross-stratification (facies Sl(e)) and isolated sets or co-sets of trough cross-bedding (facies St(e)). Internally, the foresets of St(e) and Sl(e) are composed of millimetrically spaced laminations characterized by bimodal, inversely graded pinstripe. In some cases, crenulated horizontal laminae (Sa(e)) are described within low-angle cross-stratification facies. From a view parallel to palaeoflow, tangential cross-strata contain bounding surfaces that truncate underlying cross-strata, they are inclined at 7° and have a lateral spacing of 1,5 m. The overlying cross-stratification planes are either concordant with the bounding surfaces or exhibit downlap.

Interpretation: The very fine-to medium-grained sandstones with horizontal or low-angle cross-stratification, composed exclusively of wind-ripple lamination, are interpreted as eolian sandsheets deposits (Hunter, 1977; Kocurek and Nielson, 1986; Scherer, 2000). These sandsheets are dominated by translantent wind ripples associated with eolian bedform migration under wind transport in drier contexts, and adhesion structures related to wetter climatic conditions. The occurrence of well-sorted sandstones organized into isolated sets or co-sets of trough cross-bedding, composed of wind-ripple laminae suggest deposition as eolian dunes. The occurrence of translantent wind-ripple laminae indicates that many dunes either lacked a significant active lee-side slipface. The bounding surfaces that overlying cross-stratification planes, either concordant with the bounding surfaces or into downlap are reactivation surfaces. These erosional surfaces resulting from fluctuating airflow on the lee slope of an active bedform (Brookfield, 1977).

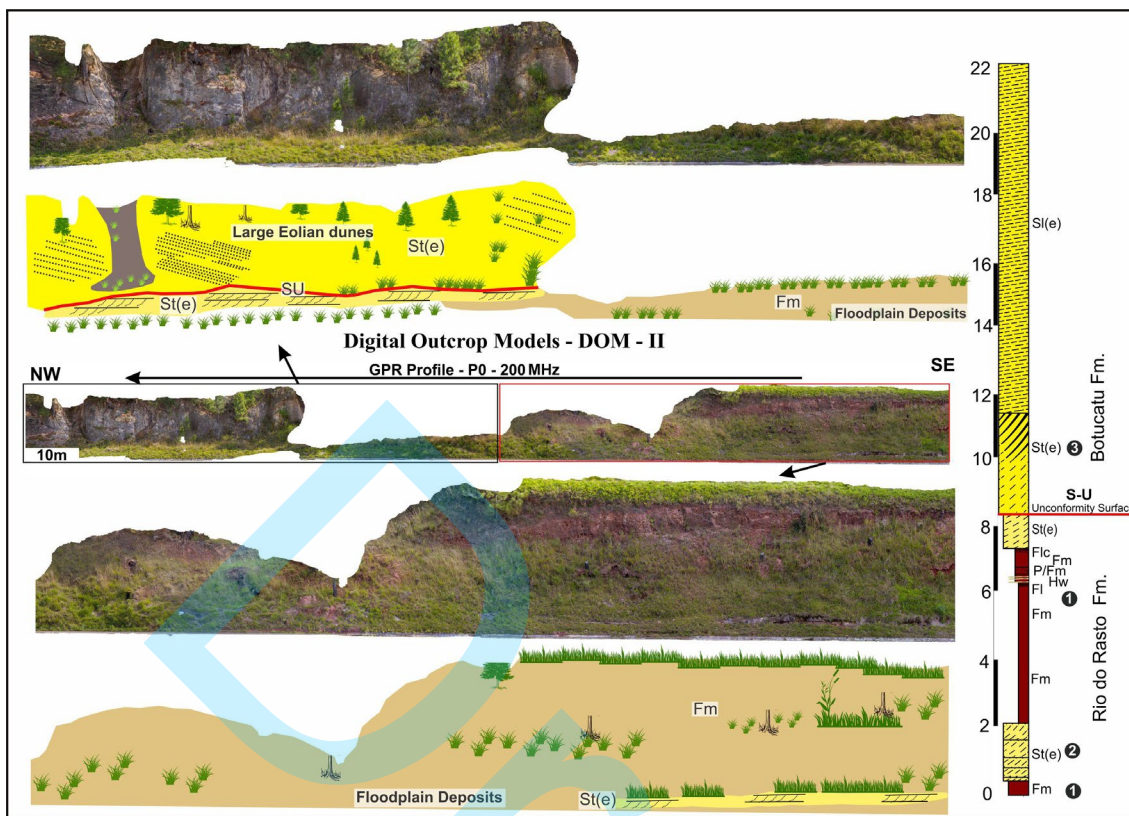


Figure 7. Stratigraphic cross-section (NW-SE) based on panel from the central section (PRR020). This sequence is composed by eolian sand sheets and eolian dune field interbedded ephemeral lacustrine deposits. The numbers 1, 2 and 3 indicate the individual architectural elements.



Figure 8. Stratigraphic cross-section (NW-SE) based on panel from the central section (PRR022). This sequence is composed by eolian sand sheets, and large eolian dunes. The S-U represents the unconformity surface between the Rio do Rasto and Botucatu Fm. The numbers 1, 2 and 3 indicate the individual architectural element described in the Figure 7.

Botucatu Formation: Large Eolian Dunes

Description: These deposits consist of fine-to coarse-grained sandstones that are well-sorted, with subrounded to rounded grains, arranged in cross-stratified sets. Individual sets are up to 10 m, **Figure 9**. In orientations transverse to paleoflow, simple sets of cross-bedding and their basal bounding surfaces reveal trough-shaped element geometries, **Figure 5**, troughs are 56 m wide. By contrast, in orientations parallel to the direction of dip of the cross-strata, inclined cross-bedding is tangential to basal set bounding surface, **Figure 5**. Internally, foresets within sets have uppermost parts that are composed of massive sandstone or inversely-graded grainflow lenses that dip at 22°. Toeset deposits are characterized by inversely graded wind-ripple laminae. Internally, the cross-bedded sets can be subdivided into sub-sets bounded by surfaces that truncate the strata below, whereas the strata above are concordant with the dipping bounding surfaces. The dipping bounding surfaces are themselves inclined up to 19°. Foreset dip azimuths are variable in the range to 22° to 25°.

Interpretation: the medium-to large scale cross-strata sandstones compounded by grain flow and wind-ripple strata are interpreted as formed by the migration of large eolian dunes. The presence of grainflow strata indicates high-angle, well-developed slipfaces (Hunter, 1977). The unimodal trend of the cross-bed dip azimuths, and their occurrence in trough-shaped sets indicates crescentic dunes with sinuous crestlines (Rubin and Hunter, 1982). The concave-up surfaces that truncate the foresets are interpreted as reactivation surfaces, which reflect frequent changes in the wind flow.

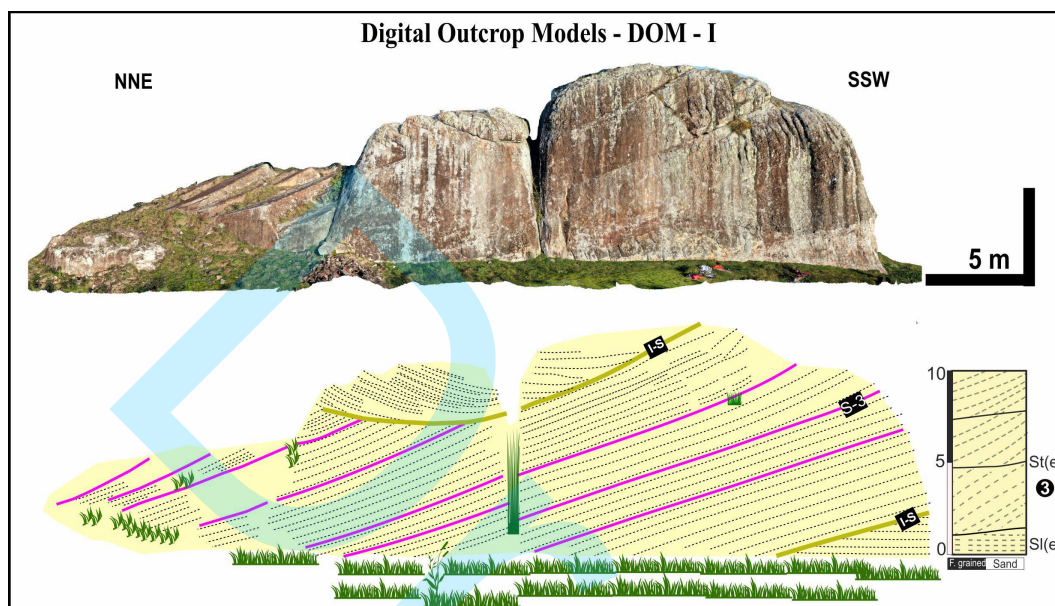


Figure 9. Stratigraphic cross-section (NNE-SSW) based on panel from the central section (BT-15). This sequence is composed by set of cross-strata formed by facies (ST(e)). Note that first-order surfaces (I-S) separate sets of sandstones with large cross-bedding and third-order surfaces (S-3) occur internally within the sets, truncating the adjacent strata. The number 3 indicates the architectural element.

AQUIFERS HETEROGENEITIES

The reservoirs that make up the studied interval are predominantly composed of fine-to coarse-grained sandstones that are moderately to well-sorted, and which were deposited by dry eolian and fluvial-eolian systems. These deposits juxtapose vertically and laterally, generating a highly complex depositional architecture, within which multiple scales of heterogeneity are present. In this sense, heterogeneities of eolian reservoirs have been analyzed at seismic scale, considering the decametric and kilometric compartmentalization of eolian reservoirs (e.g Taggart et al., 2010); II) at decametric scale including the diagenetic heterogeneities due to the growing of giant calcite concretions which geometry is controlled by eolian bounding surfaces (Arribas et al., 2012); and III) at lamina scale where grain flow laminae typically exhibit permeability of an order of magnitude greater than the grain-fall and wind-rippled strata which encase them (Howell and Mountney, 2001). Rodríguez-López and Wu, 2020) also add that syndimentary mass-wasting deformations in the eolian dune sands as well constitute relevant heterogeneities in eolian reservoir. Based on the classification of Galloway and Hobday (1996), the

studied stratigraphic interval can be subdivided on three heterogeneity scales: megascopic, macroscopic and mesoscopic heterogeneity.

Megascopic Heterogeneity

Megascopic Heterogeneity describes the geometry, lateral continuity and vertical communication of the reservoir layers. Bongiolo and Scherer (2010) also highlight that at this scale the main parameters controlling reservoir compartmentation are the key stratigraphic surfaces;

The lower and middle intervals of the Rio do Rasto Formation are composed of more compartmentalized reservoirs of thinner eolian packages that are laterally discontinuous, reflecting fluvial dynamics. These reservoirs generate a very complex stratigraphy due to the vertical and lateral juxtaposition of fluvial and eolian sand bodies. The main flow barriers in this interval are represented by the silt clay layers and the unconformity surface (S-U) identified in the radargrams and in DOM II, **Figure 8**. In contrast, the upper interval is composed of thick packages of eolian sandstone (Botucatu Fm.) with relatively simple lateral continuity due to the tabular geometry of the sand bodies, **Figure 10**. From the perspective of the characterization of eolian reservoirs, these bounding surfaces identified in both radargrams and DOM can act as barriers to fluid migration, exhibiting prominent contrasts in grain size (e.g., Shebi, 1995; Ciftci et al., 2004). Bounding surfaces can also transmit percolating meteoric waters, resulting in the upgrading of carbonate and silicate cements (e.g., Chandler et al., 1989; North and Prosser, 1993), and the alteration of other diagenetic processes, such as mechanical compaction, infiltration of clays and chlorite cementation (e.g. Bongiolo and Scherer, 2010; De Ros and Scherer, 2013).

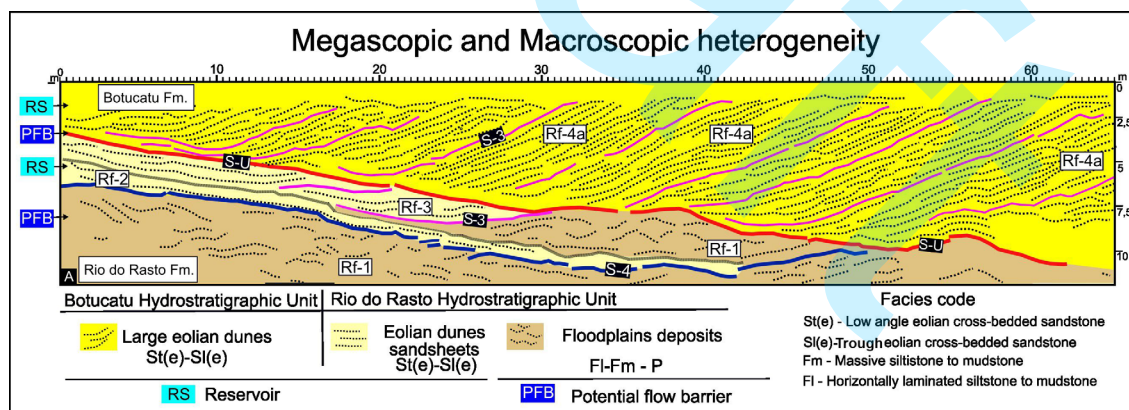


Figure 10. Simplified scheme of megascopic heterogeneity, highlighting the main elements that can act as potential flow barriers (clay layers and the unconformity surface (S-U)) and reservoirs (sandy deposits).

Macroscopic Heterogeneity

Macroscopic heterogeneity reflects vertical and lateral relationships between the facies association within the reservoir, **Figure 10**. To infer the average permeability values of facies associated with eolian

and fluvial environments, literature data was used summarized in the **Table 3**. The high permeability of the eolian dune facies (Botucatu Fm.) can be explained by Grain-flow strata display significantly higher porosity values than wind-ripple deposits, due to granulometric sorting and looser packing of grain-flow deposits in comparison to wind-ripple deposits (Chandler et al., 1989).

The eolian dune and eolian sand sheet facies associations have higher permeability (K) and porosity (Φ) values than fluvial facies association. Based on this data, it is assumed that the Morro Pelado Member (Rio do Rasto Fm.) presents lower permeability values, which can be explained by their finer grain size and presence of carbonate cements and cutan of illite/illite-smectite, chlorite and, possibly, ferrous smectite (nontronite) around the sandstone grains of the unit as described by Schemiko et al (2014). In this case, when cemented (especially by carbonates or evaporites), these deposits can form flow barriers or isolate productive strata (Ahlbrant and Frybergger, 1981; Galloway and Hobday, 1996). The high permeability of the eolian dune facies (Botucatu Fm.) can be explained by grain-flow strata display significantly higher porosity values than wind-ripple deposits, due to granulometric sorting and looser packing of grain-flow deposits in comparison to wind-ripple deposits (Chandler et al., 1989).

Table 3. Average porosity and permeability values in eolian and fluvial facies.

Facies Association	Facies	Porosity and Permeability	References
Eolian	Eolian dune	Φ : 16,3% kh: 137 - 154 mD kv: 200 mD	Lindquist (1998) Nugget Fm.
Eolian	Interdune	Φ : 2,3% kh: 0,01 - 0,02 mD kv: 0,01 mD	
Eolian	Eolian dune	Φ : 15,3% k average: 64,79 mD	Bongiolo and Scherer (2010) Sergi Fm.
Eolian	Eolian sand sheets	Φ : 12,7% k average: 44,1 mD	
Fluvial	Fluvial channel	Φ : 9,1% k average: 3 mD	
Eolian	Eolian dune – deposition under conditions of high water table	Φ : 11% kh: 0,033 - 0,45 mD kv/kh: 1 mD	Taggart et al. (2010) Rotliegend Gp.
Fluvial	Massive eolian sandstone – Fluvial channel-fill deposits	Φ : 13 - 15% kh: 0,062 – 3,2 mD kv/kh: 0,18 mD	
Fluvial	Overbank deposits	Φ : 11% kh: 0,33 – 0,45 mD kv/kh: 1 mD	
Eolian	Eolian dune	Φ : 31% k average: 151 mD	Wojahn (2011) Botucatu Fm.

Mesosopic Heterogeneity

Individual eolian and fluvial packages possess internal textural and structural differences that account for changes in petrophysical features of the reservoirs (mesoscopic heterogeneity). Fluvial facies association show variable permoporosity values, adopted for this study, **Table 3**, Lithofacies St(e), Sl(e) (upper portions predominantly) have higher permeabilities than lithofacies Fm and Fl (bottom portions respectively). Lower permeability values of lithofacies Fm/Fl can be explained by its finer grain-size, whereas those of lithofacies St(e), Sl(e) and presence of carbonate cements from lithofacies Fm/Fl can generate effective flow barriers that yield the compartmentalization of fluvial-eolian reservoirs.

The eolian dune facies association comprises dominantly superposing sets of the eolian cross-strata lithofacies St(e). At the base of the foreset, strata are tangential to the underlying bounding surface and are characterized by wind-ripple lamination. The upward steepening of foreset inclination within sets and their association with the occurrence of inversely graded grain-flow strata is usually accompanied by permeability changes, which tend to condition the flow according to this change, **Figure 11**.

This change in the eolian stratification type along the foresets is usually accompanied by permeability changes (e.g. Lindquist, 1988; Chandler et al., 1989; Howell and Mountney, 2001). Grain-flow strata display significantly higher porosity values than wind-ripple deposits, due to granulometric sorting and looser packing of grain-flow deposits in comparison to wind-ripple deposits (Chandler et al., 1989). These differences in permeability at the base and top of cross-strata influence the preferred direction of fluid flow and should be considered when developing reservoir models, as argued by Chandler et al. (1989) and Howell and Mountney (2001).

Lithologic and Aquifer Model

From a hydrostratigraphic point of view, one of the first steps to implement the classification of aquifer systems was to identify the lithological units in the in the data collected and presented previously. Based on this and considering that stratigraphic units consist of one or more lithological units interrelated in vertical succession, which have similar textural characteristics and are associated with the same type of depositional environment, it was possible to identify two hydrostratigraphic units in the area, Botucatu and Rio do Rasto Formation, which are associated in this work with aquifer 1 - unconfined and aquifer 2 - Confined, respectively, **Figure 11 A, B and C**.

The analysis of the data presented suggests that the Rio do Rasto hydrostratigraphic Unit behaves as an irregular or multi-layered aquifer reservoir that exhibits jigsaw puzzle-type geometry, according to the classification of Weber and Van Geuns (1990), in which the intercalations of sandy layers and silt-clay beds affect hydraulic continuity, **Figure 10**. On the other hand, the Botucatu hydrostratigraphic unit presents a Layer Cake reservoir. This style is characterized by presenting lateral continuity and relatively simple correlation, **Figure 11 E**. This definition is in line with the 3D models presented, in which the Botucatu hydrostratigraphic unit is of the tabular and continuous type.

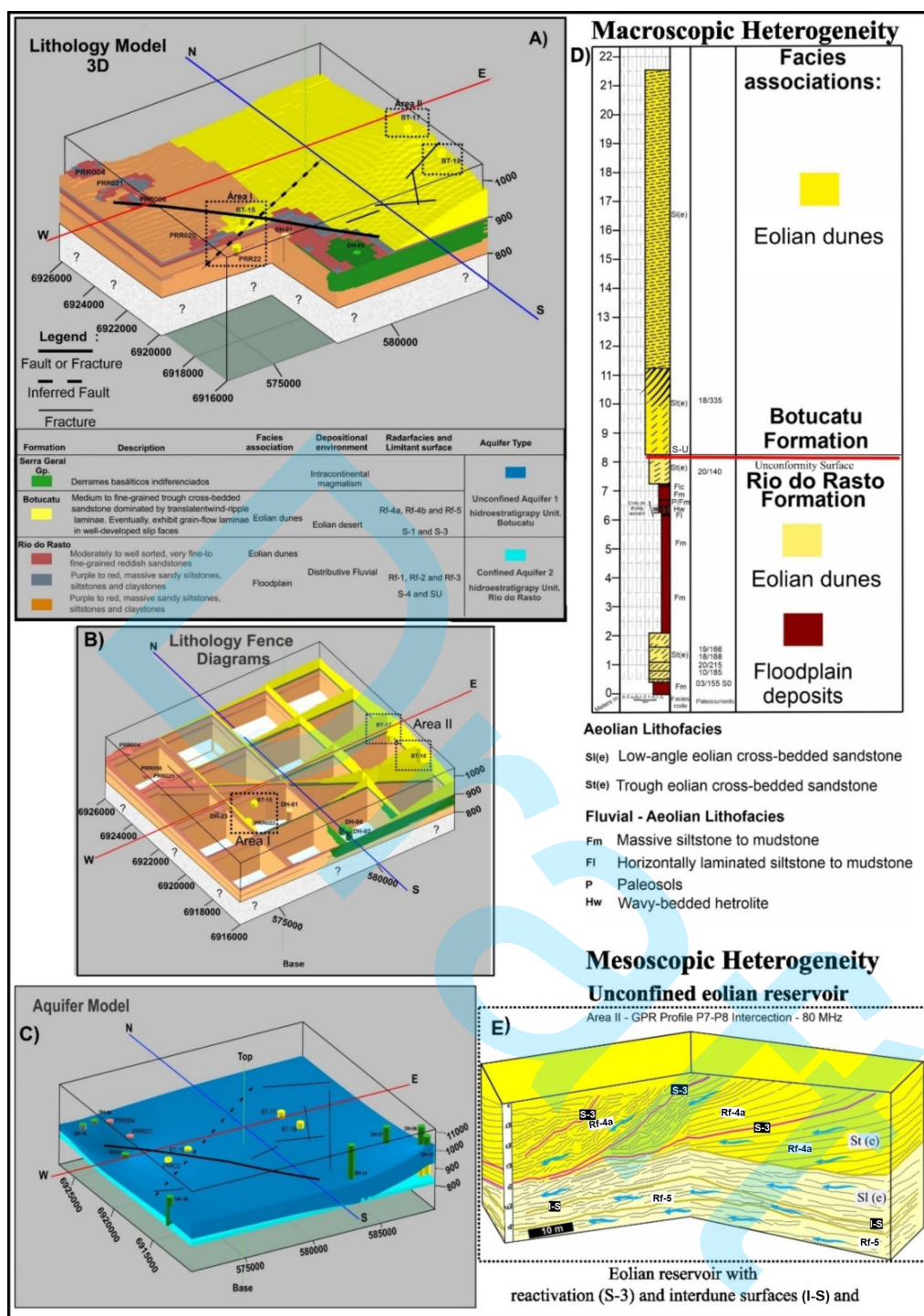


Figure 11. A) lithologic model showing the three-dimensional representation of the sedimentary system; B) Fence diagram exhibiting internal lateral and vertical variations of lithofacies; C) Aquifer model showing the 3D representation of aquifers unconfined (upper portion) and confined (lower portion); D) Simplified scheme of megascopic heterogeneity; E) Simplified scheme of mesoscopic heterogeneity showing the preferential direction of flow in eolian facies. E) Expected scenario of a conceptual wind reservoir presenting different sedimentary heterogeneities and preferential flow directions.

CONCLUSIONS

The reservoirs that make up the studied interval are originated by two distinct depositional systems: the first Morro Pelado Member (Rio do Rasto Fm.) is predominantly composed of dominated by lithofacies of the floodplain deposits include dominantly red to purple massive and blocky to horizontally laminated fine-grained rocks (Fm and Fl, respectively). Interbedded by moderately to well-sorted, very fine-to medium-grained sandstones (St(e) and Sl(e)), deposited by fluvial - eolian systems. The second (Botucatu Fm.) is composed by eolian sandstone varies from fine to coarse-grained (St(e) and (Sl(e)) and often exhibit pin-stripe lamination and grain flow lenses, deposited by dry eolian systems.

Based on the facies architecture and high-resolution geophysical data, in cm scale, from the deposits of the Morro Pelado Member (Rio do Rasto Fm.) and the Botucatu Fm. and it was possible to determine the main parameters responsible for influencing the properties of reservoirs associated with the fluvial-eolian and dry eolian systems and recognize a variety of barriers to flow at different scales. At megascopic scale, the main parameters controlling reservoir compartmentalization and represent potential flow barriers, in this context, are the key-stratigraphic surfaces, unconformity surface (S-U) and the layers of clay and silt present in the Rio do Rasto Fm., which have low porosity and permeability.

Based on geometric relationships, reservoirs linked to fluvial-eolian interaction form two types in macroscopic heterogeneity: (i) highly compartmentalized eolian packages, which are truncated by fluvial deposits, and complex stratigraphic correlation and (ii) good lateral continuity of eolian packages and correlation relatively simple stratigraphy. The facies architecture in the eolian-fluvial deposits identified in the Morro Pelado Member (Rio do Rasto Fm.) is more complex, because it contains alternating intervals of eolian sandstone and fluvial heterolithic strata, both of which can be laterally discontinuous on the length scales studied. In this case, the eolian sandstone bodies surrounded by fluvial heterolithic strata can form small isolated flow units.

Furthermore, the cm scale individualization of the radarfacies corroborates the hypothesis that the Rio do Rasto hydrostratigraphic unit behaves as an irregular or multi-layered aquifer reservoir that exhibits jigsaw puzzle-type geometry, and the Botucatu hydrostratigraphic unit presents a Layer Cake reservoir, according to the classification of Weber and Van Geuns (1990).

ACKNOWLEDGMENTS

This work was financially supported by FAPESC - Foundation for Research and Innovation of the State of Santa Catarina [N° 2021TR000670 and N° 2021TR000319]. We also thank the Postgraduate Program in Geology and Federal University of Santa Catarina. We also appreciate the two anonymous reviewers for their constructive suggestions that improved the manuscript greatly.

REFERENCES

- Alessandretti, L., Warren, L. V., Machado, R., Novello, V. F., and Sayeg, I. J. 2015. Septarian carbonate concretions in the Permian Rio do Rasto Formation: birth, growth and implications for the early diagenetic history of southwestern Gondwana succession. *Sedimentary Geology*, 326, 1-15. DOI: 10.1016/j.sedgeo.2015.06.007.
- Ahlbrandt, T. S; Fryberger, S. G. 1981. Sedimentary features and significance of interdune deposits. In: *Recent and Ancient Non-Marine Depositional Environments: Models for Exploration* (Eds F.G. Ethridge and R.M. Flore), SEPM. Spec. Publ., 31, 293–314. DOI: 10.2110/pec.81.31.0293.
- Araújo L. M., França A. B., Potter P.E. 1995. Aquífero Gigante do Mercosul no Brasil, Argentina, Uruguai e Paraguai; Mapas Hidrogeológicos das Formações Botucatu, Pirambóia, Rosário do Sul, Buena Vista, Misiones e Tacuarembó. Curitiba, UFPR PETROBRAS, Map scale 1:2.500.000.
- Arribas, M. E., Rodríguez-López, J. P., Meléndez, N., Soria, A. R., and de Boer, P. L. 2012. Giant calcite concretions in eolian dune sandstones; sedimentological and architectural controls on diagenetic heterogeneity, mid-Cretaceous Iberian Desert System, Spain. *Sedimentary Geology*, 243, 130-147. DOI: 10.1016/j.sedgeo.2011.10.011.
- Azevedo, K. L. 2018. Novos Registros de Temnospondyli do Sítio São Jerônimo da Serra da Formação Rio do Rasto (Permiano/Médio Superior) do Estado do Paraná Brasil: Implicações Taxômicas, Tafonômicas, Paleoambientais e Bioestratigráficas. PhD Thesis. Universidade Federal do Rio Grande do Sul - UFRGS, Porto Alegre, RS, Brazil.
- Bállico, M.B., Scherer, C.M. S., Mountney, N.P., Souza, E.G., Reis, A.D., Gabaglia, G.R., Magalhães, A.J.C. 2017. Sedimentary cycles in a mesoproterozoic eolian erg-margin succession: Mangabeira Formation, Espinhaço Supergroup, Brazil. *Sedimentary Geology*, v. 349,1-14. Elsevier BV. DOI: [10.1016/j.sedgeo.2016.12.008](https://doi.org/10.1016/j.sedgeo.2016.12.008).
- Bergamaschi, S. 1999. Análise estratigráfica do Siluro-Devoniano (Formações Furnas e Ponta Grossa) da sub-bacia de Apucarana, Bacia do Paraná, Brasil.
- Bongiolo, D. E., Scherer, C. M. 2010. Facies architecture and heterogeneity of the fluvial–eolian reservoirs of the Sergi Formation (Upper Jurassic), Recôncavo Basin, NE Brazil. *Marine and Petroleum Geology*, 27(9), 1885-1897. DOI: 10.1016/j.marpetgeo.2010.07.015.
- Bigarella, J. J. and Salamuni, R. 1961. Early Mesozoic wind patterns as suggested by dune bedding in the Botucatu Sandstone of Brazil and Uruguay. *Geological Society American Bulletin*. 72, p.1089-1106. DOI: 10.1130/0016-7606(1961)72[1089:EMWPAS]2.0.CO;2.
- Botha, G. A., Bristow, C. S., Porat, N., Duller, G., Armitage, S. J., Roberts, H. M., Clarke, B. M; Kota, M.W. and Schoeman, P. 2003. Evidence for dune reactivation from GPR profiles on the Maputaland coastal plain, South Africa. *Geological Society, London, Special Publications*, 211(1), 29-46. DOI: 10.1144/GSL.SP.2001.211.01.03.
- Bristow, C. S.; Chroston, P. N; Bailey, S. D. 2000. The structure and development of foredunes on a locally prograding coast: insights from ground-penetrating radar surveys, Norfolk, UK. *Sedimentology*, 47 (5), 923-944. DOI: 10.1046/j.1365-3091.2000.00330.x.
- Bristow, C. S.; Lancaster, N.; Duller, G. A. T. 2005. Combining ground penetrating radar surveys and optical dating to determine dune migration in Namibia. *Journal of the Geological Society*, 162 (2), 315-321. Geological Society of London. DOI: [10.1144/0016-764903-120](https://doi.org/10.1144/0016-764903-120).
- Bristow, C; Pugh, J; Goodall, T. 1996. Internal structure of eolian dunes in Abu Dhabi determined using ground-penetrating radar. *Sedimentology*, 43 (6) 995-1003. DOI: 10.1111/j.1365-3091.1996.tb01515.x.
- Brookfield, M. E. 1977. The origin of bounding surfaces in ancient eolian sandstones. *Sedimentology*, 24 (3), p. 303-332. DOI: 10.1111/j.1365-3091.1977.tb00126.x.

- Cartigny, M. J., Ventra, D., Postma, G., and van Den Berg, J. H. 2014. Morphodynamics and sedimentary structures of bedforms under supercritical-flow conditions: new insights from flume experiments. *Sedimentology*, 61(3), 712-748. DOI:10.1111/sed.12076.
- Chandler, M. A., Kocurek, G., Goggin, D. J., Lake, L. W. 1989. Effects of stratigraphic heterogeneity on permeability in eolian sandstone sequence, Page Sandstone, Northern Arizona. *AAPG Bulletin*, 73 (5), 658-668. DOI: 10.1306/44B4A249-170A-11D7-8645000102C1865D.
- Ciftci, B. N., Aviantara, A. A., Hurley, N. F., and Kerr, D. R. 2004. Outcrop-based three-dimensional modeling of the Tensleep sandstone at Alkali Creek, Bighorn Basin, Wyoming. DOI: 10.1306/M80924C12.
- Clemmensen, L. B. 1989. Preservation of interdune and plinth deposits by the lateral migration of large linear dunes (Lower Permian Yellow Sands, northeast England). *Sedimentary Geology*, 65(1-2), 139-151. DOI: 10.1016/0037-0738(89)90011-0.
- Davis, J. L.; Annan, A. P. 1989. Ground-Penetrating Radar For High-Resolution Mapping of Soil And Rock Stratigraphy. *Geophysical Prospecting*, 37 (5) 531-551. Wiley. DOI: 10.1111/j.1365-2478.1989.tb02221.x.
- De Oliveira, M. A., Santos, J. C., and Lemos, R. 2020. 80,000 years of geophysical stratigraphic record at the Serra da Capivara National Park, in northeastern Brazil: Uncovering hidden deposits and landforms at a canyon's floor. *Journal of South American Earth Sciences*, 104, 102691.: DOI: [10.1016/j.jsames.2020.102691](https://doi.org/10.1016/j.jsames.2020.102691).
- Da Silva, F. G., and Scherer, C. M. D. S. 2000. Fácies, Associação de Fácies e Modelo Depositional dos Arenitos Eólicos da Formação Botucatu (Cretáceo Inferior) na Região Sul de Santa Catarina. *Pesquisas em Geociências*, 27 (2), 15-30. DOI: 10.22456/1807-9806.20187.
- De Ros, L. F., and Scherer, C. M. 2013. Stratigraphic Controls on the Distribution of Diagenetic Processes, Quality and Heterogeneity of Fluvial-Aeolian Reservoirs from the Recôncavo Basin, Brazil. in: Morad, S. Ketzer J.M. and Ros, L.F. De. eds., *Linking Diagenesis to Sequence Stratigraphy*, 105-132. DOI: <https://doi.org/10.1002/9781118485347.ch5>.
- Eltom, H. A., Kubur, A. K., Abdulraziq, A. M., Babalola, L. O., Makkawi, M. H., and Abdullatif, O. M. . 2017. Three-dimensional outcrop reservoir analog model: A case study of the Upper Khuff Formation oolitic carbonates, Central Saudi Arabia. *Journal of Petroleum Science and Engineering*, 150,115-127. DOI: [10.1016/j.petrol.2016.11.035](https://doi.org/10.1016/j.petrol.2016.11.035).
- Fielding, C. R. 2006. Upper flow regime sheets, lenses and scour fills: extending the range of architectural elements for fluvial sediment bodies. *Sedimentary Geology*, 190(1-4), 227-240. DOI: 10.1016/j.sedgeo.2006.05.009.
- Forte, E., Pipan, M., Casabianca, D., Di Cuia, R., and Riva, A. 2012. Imaging and characterization of a carbonate hydrocarbon reservoir analogue using GPR attributes. *Journal of Applied Geophysics*, 81, 76-87. DOI: [10.1016/j.jappgeo.2011.09.009](https://doi.org/10.1016/j.jappgeo.2011.09.009).
- Fryberger, S. G., Al-Sari, A. M., and Clisham, T. J. 1983. Eolian dune, interdune, sand sheet, and siliciclastic sabkha sediments of an offshore prograding sand sea, Dhahran area, Saudi Arabia. *AAPG Bulletin*, 67 (2), 280-312. DOI: 10.1306/03B5ACFF-16D1-11D7-8645000102C1865D.
- Galloway, W. E., Hobday D. K. 1996. Facies characterization of reservoirs and aquifers. terrigenous clastic depositional systems. Springer, Berlin, Heidelberg, p. 426-444. DOI: 10.1007/978-3-642-61018-9_16.
- Gordon Jr., M. 1947. Classificação das Formações Gonduânicas do Paraná, Santa Catarina e Rio Grande do Sul. *Boletim DNPM - DGM*, Rio de Janeiro, 38, 20.
- Gulliford, A. R., Flint, S. S., and Hodgson, D. M. 2017. Crevasse splay processes and deposits in an ancient distributive fluvial system: the lower Beaufort Group, South Africa. *Sedimentary Geology*, 358,

1-18. DOI: 10.1016/j.sedgeo.2017.06.005.

Holz, M., França, A. B., Souza, P. A., Iannuzzi, R., and Rohn, R. 2010. A stratigraphic chart of the Late Carboniferous/Permian succession of the eastern border of the Paraná Basin, Brazil, South America. *Journal of South American Earth Sciences*, 29 (2), 381-399. DOI: 10.1016/j.jsames.2009.04.004.

Howell, J., and Mountney, N. 2001. Aeolian grain flow architecture: hard data for reservoir models and implications for red bed sequence stratigraphy. *Petroleum Geoscience*, 7(1), 51-56. DOI: 10.1144/petgeo.7.1.51.

Howell, J. A.; Martinius, A. W.; Good, T. R. 2014. The application of outcrop analogues in geological modelling: a review, present status and future outlook. Geological Society, London, Special Publications, 387 (1), 1-25. DOI: [10.1144/sp387.12](https://doi.org/10.1144/sp387.12).

Hunter, R. E. 1977. Basic types of stratification in small eolian dunes. *Sedimentology*, 24, 3), 361-387. DOI: 10.1111/j.1365-3091.1977.tb00128.x.

Kocurek, G. 1991. Interpretation of ancient eolian sand dunes. *Annual Review of Earth and Planetary Sciences*, 19 (1), 43-75. DOI: 10.1146/annurev.ea.19.050191.000355.

Kocurek, G., and Hunter, R. E. 1986. Origin of polygonal fractures in sand, uppermost Navajo and Page Sandstones, Page, Arizona. *Journal of Sedimentary Research*, 56 (6), 895-904. DOI: 10.1306/212F8A7B-2B24-11D7-8648000102C1865.

Kocurek, G., and Nielson, J. 1986. Conditions favourable for the formation of warm-climate aeolian sand sheets. *Sedimentology*, 33(6), 795-816. DOI: 10.1111/j.1365-3091.1986.tb00983.x.

Kocurek, G., and Fielder, G. 1982. Adhesion structures. *Journal of Sedimentary Research*, 52(4), p. 1229-1241. DOI: 10.1306/212F8102-2B24-11D7-8648000102C1865D.

Kroth, M. 2018. Modelos virtuais de afloramento aplicados à estratigrafia de sequências e modelagem de análogos de reservatório fluvial na Bacia Lusitânica. Universidade Federal do Pampa - UNIPAMPA. Caçapava do Sul, RS, Brazil, p. 78

Lavina E. L. 1991. Geologia Sedimentar e Paleogeografia do Neopermiano e Eotriássico (Intervalo Kazaniano - Citiano) da Bacia do Paraná. PhD Thesis. Instituto de Geociências, Universidade Federal do Rio Grande do Sul - UFRS, Rio Grande do Sul, Brazil, p.248.

Lee, K., Tomasso, M., Ambrose, W. A., and Bouroulllec, R. 2007. Integration of GPR with stratigraphic and lidar data to investigate behind-the-outcrop 3D geometry of a tidal channel reservoir analog, upper Ferron Sandstone, Utah. *The Leading Edge*, 26 (8), 994-998. DOI: 10.1190/1.2769555.

Lindquist, S. J. 1988. Practical characterization of eolian reservoirs for development: Nugget Sandstone, Utah—Wyoming thrust belt. *Sedimentary Geology*, 56 (1-4), 315-339. DOI: 10.1016/0037-0738(88)90059-0.

Magalhães, A. J. C., Lima-Filho, F. P., Guadagnin, F., Silva, V. A., Teixeira, W. L. E., Souza, A. M., Raja Gabaglia G. P. and Catuneanu, O. 2017. Ground penetrating radar for facies architecture and high-resolution stratigraphy: Examples from the Mesoproterozoic in the Chapada Diamantina Basin, Brazil. *Marine and Petroleum Geology*, 86, 1191-1206. DOI: 10.1016/j.marpetgeo.2017.07.027.

Machado, J. L. F. 2013. Mapa hidrogeológico do estado de Santa Catarina. Porto Alegre: CPRM - ISBN 978-85-7499-208-2.

Marriott, S. B., and Alexander, J. (Eds.). 1999. Floodplains: interdisciplinary approaches. Geological Society of London. Special Publication n. 163. 284 pp.

Massaro, L., Corradetti, A., Vinci, F., Tavani, S., Iannace, A., Parente, M., and Mazzoli, S. 2018. Multiscale fracture analysis in a reservoir-scale carbonate platform exposure (Sorrento Peninsula, Italy): implications for fluid flow. *Geofluids*. 1-10. DOI: 10.1155/2018/7526425.

- Meghlhioratti, T. 2006 *Estratigrafia De Sequências das Formações Serra Alta, Teresina e Rio Ddo Rasto (Permiano, Bacia do Paraná) na Porção Nordeste do Paraná e Centro-Sul de São Paulo*. PhD Thesis. Instituto de Geociências e Ciências Exatas, Universidade Estadual Paulista, Rio Claro, SP, Brazil, p. 134.
- Miall, A. D. 1996. *The Geology of Fluvial Deposits: Sedimentary Facies, Basin Analysis, and Petroleum Geology*. Springer, Berlin 582 pp.
- Milani, E. J. 1997. *Evolução tectono-estratigráfica da Bacia do Paraná e seu relacionamento com a geodinâmica fanerozóica do Gondwana sul-ocidental*. PhD Thesis. Universidade Federal do Rio Grande do Sul – UFRGS. Porto Alegre, RS, Brazil,
- Milani, E. J., Gonçalves de Melo, J. H., De Souza, P. A., Fernandes, L. A. and França, A. B. 2007. *Bacia do Paraná*. *Boletim de Geociências da Petrobras*, 15, 265–287.
- Mitchum Jr., R. M. 1977. *Seismic Stratigraphy and Global Changes of Sea Level, Part II: Glossary of Terms Used in Seismic Stratigraphy*. In: Payton, C.E. (ed.). *Seismic Stratigraphy-Applications to Hydrocarbon Exploration*. The American Association of Petroleum Geologists Memoir 26, p. 205-212. DOI: 10.1306/M26490C13.
- Mitchum, Jr. R. M; Vail, P. R; Sangree, J. B; 1977. *Seismic stratigraphy and global changes of sea level: Part 6. Stratigraphic interpretation of seismic reflection patterns in depositional sequences. Stratigraphic interpretation of seismic reflection patterns in depositional sequences* In: Payton, C.E. (Ed.), *Seismic Stratigraphy-Applications to Hydrocarbon Exploration*. AAPG Memoir 26, p. 117– 133. DOI: [10.1306/M26490C8](https://doi.org/10.1306/M26490C8).
- Mountney, N.P. 2006. *Eolian Facies Models*. In: *Facies Models Revisited* (Eds H. Posamentier and R.G. Walker). SEPM Mem., 84, p.19 – 83.
- Neal, A. 2004. *Ground-penetrating radar and its use in sedimentology: principles, problems and progress*. *Earth-Science Reviews*, 66(3-4), 261-330. DOI: 10.1016/j.earscirev.2004.01.004.
- Neal, A and Roberts, C. L. 2001. *Internal structure of a trough blowout, determined from migrated ground-penetrating radar profiles*. *Sedimentology*, 48 (4). 791-810. DOI: 10.1046/j.1365-3091.2001.00382.x.
- North, C. P., and Prosser, D. J. 1993. *Characterization of fluvial and aeolian reservoirs: problems and approaches*. Geological Society, London, Special Publications, 73(1), 1-6. DOI: 10.1144/GSL.SP.1993.073.01.01.
- Pasetto, G. A., Gonçalves, I. G., Guadagnin, F., and dos Santos, E. G. 2020. *Modelagem Geológica Implícita em Mina de Mármore no Complexo Metamórfico Passo Feio, Rio Grande do Sul, Brasil*. *Anuário do Instituto de Geociências*, 43(4), 202-217. DOI: 10.11137/2020_4_202_217.
- Plint, A. G., James, N. P., and Dalrymple, R. W. 2010. *Wave-and storm-dominated shoreline and shallow-marine systems*. *Facies models*, 4(167-201).
- Pringle, J. K., Westerman, A. R., Clark, J. D., Drinkwater, N. J., and Gardiner, A. R. 2004. *3D high-resolution digital models of outcrop analogue study sites to constrain reservoir model uncertainty: an example from Alport Castles, Derbyshire, UK*. *Petroleum Geoscience*, 10 (4), 343-352. DOI: 10.1144/1354-079303-617.
- Rebouças, A. D. C. 1976. *Recursos hídricos subterrâneos da Bacia do Paraná: Análise de pré-viabilidade*. PhD Thesis. Universidade de São Paulo – USP, São Paulo, SP, Brazil. DOI: 10.11606/T.44.2014.tde-02062014-141431.
- Reineck, H. E. and Singh, I. B. 2012. *Depositional sedimentary environments: with reference to terrigenous clastics*. Springer Science and Business Media.
- Retallack, G. J. 1976. *Triassic palaeosols in the Upper Narrabeen Group of New South Wales. Part I:*

- features of the palaeosols. *Journal of the Geological Society of Australia*, 23(4), 383-399. DOI: 10.1080/00167617608728953.
- Riccomini, C.; Sant'anna, L. G.; Tassinari, C. C. G. 2012. Pré-sal: geologia e exploração. *Revista USP*, 95, p.33-42. DOI: 10.11606/issn.2316-9036.v0i95p33-42.
- Rohn, R. *Evolução Ambiental da Bacia do Paraná durante o Neopermiano no leste de Santa Catarina e do Paraná*. São Paulo-SP. 1994. PhD Thesis. Universidade de São Paulo – USP, São Paulo, SP, Brazil. DOI: 10.11606/T.44.1995.tde-22062015-145002.
- Rodríguez-López, J. P., and Wu, C. 2020. Recurrent deformations of aeolian desert dunes in the cretaceous of the South China Block: Trigger mechanisms variability and implications for aeolian reservoirs. *Marine and Petroleum Geology*, 119, 104483. DOI: 10.1016/j.marpetgeo.2020.104483.
- Roisenberg, H. B. 2020. Modelos virtuais de afloramento: aplicação na estratigrafia de alta resolução em sistemas fluviais entrelaçados. Final work for the undergratuation. Universidade Federal de Santa Catarina – UFSC. Florianópolis, SC, Brazil.
- Rubin, D. M., and Hunter, R. E., 1982. Bedform climbing in theory and nature. *Sedimentology*, 29, 121-138. DOI: 10.1111/j.1365-3091.1982.tb01714.x.
- Scheibe, L. F. 1986. *Geologia e petrologia do distrito alcalino de Lages, SC*. PhD Thesis. Universidade de São Paulo – USP. São Paulo, SP, Brazil. DOI: 10.11606/T.44.2016.tde-16022016-131224.
- Schemiko, D. C. B., Vesely, F. F., Fernandes, L. A., and Sowek, G. A. 2014. Distinção dos elementos deposicionais fluviais, eólicos e lacustres do Membro Morro Pelado, Permiano Superior da Bacia do Paraná. *Geologia USP. Série Científica*, 14(3), 29-46: DOI: 10.5327/z1519-874x201400030003.
- Scherer, C.M.S. 1998. *Análise estratigráfica e litofaciológica da Formação Botucatu (Neocomiano) no Estado do Rio Grande do Sul*. PhD Thesis. Universidade Federal do Rio Grande do Sul – UFRS, Porto Alegre, RS, Brazil.
- Scherer, C. M. S. 2000. Eolian dunes of the Botucatu Formation (Cretaceous) in southernmost Brazil: morphology and origin. *Sedimentary Geology*, 137(1-2), 63-84. DOI: 10.1016/S0037-0738(00)00135-4.
- Shebi, M. A. 1995. The impact of reservoir heterogeneity on fluid flow in the Tensleep Sandstone of the Bighorn Basin: Resources of southwestern Wyoming, field conference guidebook: Wyoming Geological Association. *Wyoming Geol. Ass.*, 343-359.
- Soares, A. P., Soares, P. C., and Holz, M., 2008. Heterogeneidades hidroestratigráficas no sistema Aquífero Guarani. *Brazilian Journal of Geology*, 38 (4), 598-617. DOI: 10.25249/0375-7536.2008384598617.
- Souza, A. D. M. 2013. Proposta metodológica para o imageamento, caracterização, parametrização e geração de modelos virtuais de afloramentos. PhD Thesis. Universidade Federal do Rio Grande do Norte. Natal, RN, Brazil. 149 p.
- Sweet, M. L., and Kocurek, G. 1990. An empirical model of aeolian dune lee-face airflow. *Sedimentology*, 37(6), 1023-1038. DOI: 10.1111/j.1365-3091.1990.tb01843.x.
- Sweet, M. L. 1992. Lee-face airflow, surface processes, and stratification types: their significance for refining the use of eolian cross-strata as paleocurrent indicators. *Geological Society of America Bulletin*, 104(11), 1528-1538. DOI: 10.1130/0016-7606(1992)104<1528:LFASPA>2.3.CO;2.
- Taggart, S., Hampson, G. J., and Jackson, M. D. 2010. High-resolution stratigraphic architecture and lithological heterogeneity within marginal aeolian reservoir analogues. *Sedimentology*, 57(5), 1246-1279. DOI: 10.1111/j.1365-3091.2010.01145.x.
- Thomas, H., Brigaud, B., Blaise, T., Saint-Bezar, B., Zordan, E., Zeyen, H., and Mouche, E. 2021. Contribution of drone photogrammetry to 3D outcrop modeling of facies, porosity, and permeability heterogeneities in carbonate reservoirs (Paris Basin, Middle Jurassic). *Marine and Petroleum Geology*, 123, 104772. DOI: 10.1016/j.marpetgeo.2020.104772.

Toledo, J. C. 2023. Interações flúvio-eólicas no contexto fluvial distributivo da Formação Rio do Rasto (guadalupiano-lopíngiano), Bacia do Paraná. PhD Thesis. Universidade Federal de Santa Catarina – UFSC, Florianópolis, SC, Brazil.

Van, Overmeeren, R. A., 1998. Radar facies of unconsolidated sediments in The Netherlands: A radar stratigraphy interpretation method for hydrogeology. *Journal of Applied Geophysics*, 40(1-3), 1-18. DOI: 10.1016/S0926-9851(97)00033-5.

Viana, C. D., Grohmann, C. H., Busarello, M. D. S. T., and Garcia, G. P. B. 2018. Structural analysis of clastic dikes using Structure from Motion - Multi-View Stereo: A case-study in the Paraná Basin, southeastern Brazil. *Brazilian Journal of Geology*, 48(04), 839–852. DOI: 10.1590/2317-4889201800201898.

Webber K. J. and Van Geuns L. C. 1990. Framework for constructing clastic reservoir simulation models. *Journal of Petroleum Technology* 42(10), 1248-1297. DOI: 10.2118/19582-PA.

Warren, L. V., Almeida, R. P., Hachiro, J., Machado, R., Roldan, L. F., Steiner, S. D. S., and Chamani, M. A. C. 2008. Evolução sedimentar da Formação Rio do Rasto (Permo-Triássico da Bacia do Paraná) na porção centro sul do estado de Santa Catarina, Brasil. *Revista Brasileira de Geociências*, 38(2), 213-227.

Wojahn, D. 2011. Parâmetros hidrogeológicos do Sistema Aquífero Guarani na sub-bacia do Arroio Portão/RS. PhD Thesis. Universidade do Vale do Rio dos Sinos – UNISINOS, Porto Alegre, RS, Brazil.

Lemos, R.: contributed to conceptualization, investigation, coordination of field activities, data acquisition, processing and modeling in software, writing original draft preparation and review; **Bállico, M. B.:** contributed to validation, formal analysis, supervision, project administration, and final review; **De Oliveira, M.A.T:** contributed to conceptualization, investigation, coordination of field activities, data acquisition, processing, GPR software and final review; **Guadagnin, F.:** contributed to the coordination of field activities, acquisition of aerial photos with RPA; **Manna, M.O.:** Contributed to the collection of field data, discussion and presentation of results; **Metzner, M.:** Contributed to processing and interpretation of digital outcrop model; **Feitosa, A. S. C.:** Contributed to processing and interpretation of digital outcrop model; **Toledo, J.C.:** Contributed to the collection of field data, discussion and presentation of results.